x dependence of the electronic properties of cubic Na_xWO_3

T. Wolfram
Amoco Corporation, Amoco Research Center, Naperville, Illinois 60566

L. Sutcu
Department of Physics, University of Missouri—Columbia, Columbia, Missouri 65201
(Received 17 December 1984)

Analysis of a variety of experimental data for cubic Na_xWO_3 ($0.5 \leq x \leq 1$) indicates that the electronic structure changes significantly with composition x. The lower—conduction-band width decreases and the band gap increases with increasing x. A simple theoretical model is developed which describes the x dependence of the electronic properties of cubic Na_xWO_3. The model provides closed-form analytical expressions for the energy bands, and the total and partial density-of-states functions. Results are obtained for the electronic specific heat, effective mass, magnetic susceptibility, and photoemission energy distribution curves of Na_xWO_3. These results are shown to agree with experimental data much better than the results of the rigid-band model.

I. INTRODUCTION

The electronic, optical, and thermal properties of the sodium tungsten bronzes, Na_xWO_3, have been extensively investigated experimentally in recent years. Nonstoichiometric compounds can be formed for $0 \leq x \leq 1$ which display a variety of interesting, if not puzzling, x-dependent properties.

For $x < 0.24$, Na_xWO_3 is believed to be a Mott-type insulator.[1–3] For $0.24 < x < 0.49$, Na_xWO_3 is a superconductor with a tetragonal structure.[4–6] In the range $0.5 \leq x \leq 1$, Na_xWO_3 is metallic and has the simple-cubic perovskite structure.[7,8] This paper is concerned with the properties of Na_xWO_3 in the latter range where the structure is cubic.

A large number of experiments providing x-ray photoelectron spectroscopy (XPS) and ultraviolet photoelectron spectroscopy (UPS) photoemission data,[9–16] optical data, electronic data,[16–32] specific-heat data,[26,32] and magnetic susceptibility data[28,32] have been reported for cubic metallic Na_xWO_3.

In contrast to the experimental situation, very little theoretical work exists concerning the x-dependent properties of Na_xWO_3. Calculations by Kopp, Harmon, and Liu[33] appear to be the only quantitive band structure that has been reported. These authors calculated the energy bands for (hypothetical) cubic WO_3 and for cubic $NaWO_3$ using a non-self-consistent, nonrelativistic version of the Korringa-Kohn-Rostoker (KKR) method. They reported that the band structures of these two limiting cases of Na_xWO_3 were nearly identical and concluded that a rigid-band model (RBM) was valid for describing the x dependence of the electronic properties of Na_xWO_3 in the cubic range. According to the RBM the band structure is independent of x and the (fixed) conduction-band states are progressively filled as x increases.

Calculations of the electronic specific heat[12] and the magnetic susceptibility based on a RMB density of states (DOS) do not agree well with the experimental data. Based on optical measurements, Owen *et al.*[18] have argued that the band gap of cubic Na_xWO_3 increases about 0.5 eV in going from $x = 0.52$ to $x = 0.94$, but they nevertheless state that the Na_xWO_3 system exhibits almost rigid-band behavior.

A number of photoemission results reported recently have led to a controversy concerning the validity of the RBM for cubic Na_xWO_3. Höchst *et al.*[11,12] carried out UPS photoemission measurements for samples covering the entire x range. They reported that the width of the filled portion of the conduction band remains approximately constant with x, a result that is in direct conflict with the predictions of the RBM. On the other hand, Wertheim and Chazalviel[10] argued that the results of Höchst *et al.* were erroneous and concluded that there are no data which contradict rigid-band behavior for cubic Na_xWO_3. Hollinger *et al.*[13] also concluded from their UPS data that the RBM was approximately valid. On the other hand, Egdell and Hill[14] reported UPS photoemission studies for $0.26 \leq x \leq 0.76$ and concluded that the behavior of Na_xWO_3 does *not* appear to arise from filling of a rigid conduction band.

Summarizing the above results, there appears to be considerable disagreement about the validity of the RBM for describing the x-dependent properties of cubic metallic Na_xWO_3 ($0.5 \leq x \leq 1$). Conclusions based on photoemission studies are about evenly divided on the RBM question. Authors arguing in favor of the RBM have often ignored the problem of reconciling the RBM with the electronic specific heat and magnetic susceptibility data. No quantitative theoretical calculations have dealt with the x dependence of the electronic band structure except for the end-point calculations (for $x = 0$ and $x = 1$) supplied by Koop *et al.*[33]

It seems clear that there is a real need to have a better understanding of the x-dependent properties of Na_xWO_3. A theoretical model for describing these properties which is capable of accounting for *all* of the experimental data is needed. The purpose of this paper is to present a simple model that fulfills this need.

II. QUALITATIVE DESCRIPTION OF THE ELECTRONIC STRUCTURE OF Na_xWO_3

The cubic perovskite structure is illustrated in Fig. 1. For $NaWO_3$ the W ion is situated at the center of the cubic cell (solid circle) surrounded by six oxygen ions each centered on a cube face (open circles). The sodium ions occupy the cube corners (shaded circles). For Na_xWO_3, with $0.5 \leq x \leq 1$, the Na ions are randomly distributed among the corner sites.[34]

Detailed discussions of the electronic structure of the d-band perovskites, in general,[35,36] and of $NaWO_3$ in particular,[33,37] have been presented elsewhere and only a brief description will be given here. A complete discussion of the LCAO model used in this work is available in Refs. 35 and 36.

The important energy bands are derived from the oxygen $2p$ and the tungsten $5d$ orbitals. For a unit cell, which contains three oxygen ions and one tungsten ion, there are 14 $2p-5d$ bands formed [$(3\times3=)$ 9 $2p$ orbitals plus 5 $5d$ orbitals] Nine of these bands, predominantly oxygen $2p$ orbital in character, form the valence bands. The conduction bands consist of three equivalent lower bands, the t_{2g} conduction bands, formed from an admixture of $2p$ and $5d$ orbitals having the t_{2g} symmetry. There are two upper conduction bands formed from the $2p$ and e_g-type $5d$ orbitals. The $3s$ bands associated with the Na ions lie well above the Fermi level and consequently each Na ion contributes one electron to the t_{2g} bands.

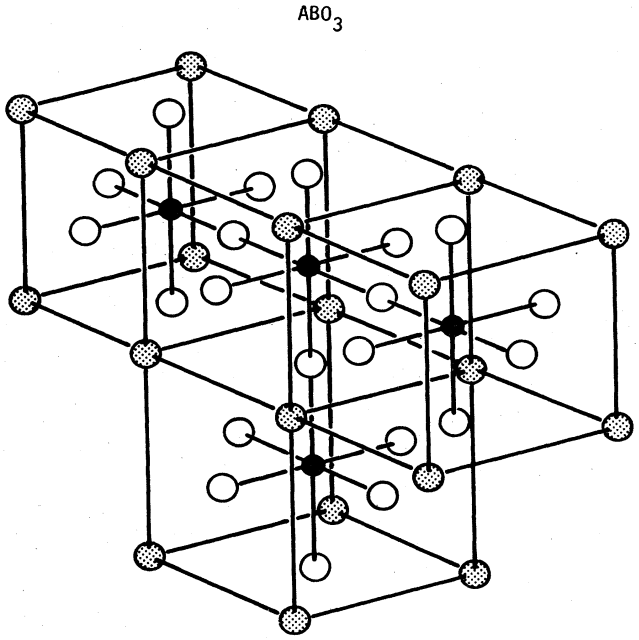

FIG. 1. Lattice structure of the ABO_3 cubic perovskite. The open circles represent oxygen ions, the solid circles indicate the transition-metal B ions (W ions), the shaded circles represent the A ions (Na ions). The lattice parameter is $2a$, where a is the B-O ion internuclear distance.

While the Na energy bands play no direct role in the electronic properties, the contribution of the Na ions to the potentials acting on the oxygen and tungsten ions is important in determining the x-dependent behavior of Na_xWO_3.

The experimetnal XPS energy distribution curve for $Na_{0.8}WO_3$ of Chazalviel *et al.*[9] is shown in Fig. 2 by the dotted curve. The emission between -12 and -4 eV arises from the valence bands. The structure between -1 eV and the Fermi level (0 eV) is due to emission from the partially filled t_{2g} conduction bands. The small emission in the band-gap region, between -4 and -1 eV, is due to plasmon effects.

Also shown in Fig. 2 are two theoretical curves.[37] The dashed curve, labeled N', is constructed from the partial density-of-states (PDOS) functions for the $2p$ and $5d$ electrons. At the high energies of XPS the photoionization cross section of the d electrons is greater than that of the p electrons by a factor of 12.[37] The N' curve consists of 12 parts d PDOS and one part p PDOS. The curve labeled $\langle N' \rangle$ is the convolution of N' with the Gaussian instrumental resolution function and should be compared with the experimental data.

The agreement between theory and experiment is good over the entire energy range but is nearly exact for the conduction-band emission. The exceptional agreement between the theory and experiment for the conduction-band intensity reflects the fact that the lower conduction bands are described exceedingly well by our LCAO theory. The remainder of this paper will be centered upon the behavior of these t_{2g} conduction bands as a function of x, the sodium concentration.

According to our LCAO model, the t_{2g} bands are described by the following equation:

$$E_{\alpha\beta}(k)=E_M+\{(E_g/2)^2+4[(pd\pi)]^2 \times[\sin^2(k_\alpha a)+\sin^2(k_\beta a)]\}^{1/2} \quad (1)$$

where $\alpha\beta=xy$, xz, and yz, k_α is the αth component of the wave vector and a is the W—O spacing. The band-

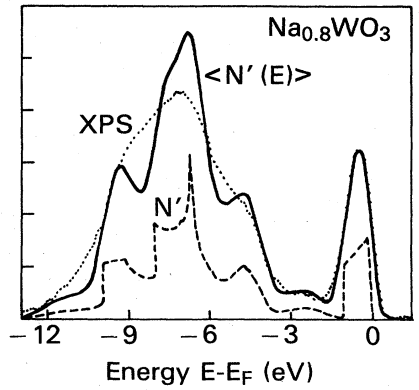

FIG. 2. Comparison of the theoretical XPS photoemission energy distribution curve with the XPS data (dots) of Ref. 9. The LCAO model employed for the theory is described in Ref. 37.

gap energy, E_g, and the midgap energy, E_M, are given by $E_g=\frac{1}{2}(E_c-E_v)$ and $E_M=\frac{1}{2}(E_c+E_v)$, where E_v and E_c are the energies of the top of the valence band and the bottom of the conduction bands, respectively. $(pd\pi)$ is the LCAO transfer integral[5] that measures the p-d—orbital interaction strength.

Each of these bands, xy, xz, and yz, depends only on two components of the three-dimensional wave vector k, and consequently each has two-dimensional characteristics which are reflected in the PDOS functions.[36,38] The DOS functions can be obtained as exact closed-form expressions:[36]

$$N(E)=\frac{6(E-E_M)}{2(pd\pi)^2}K(W(E)) , \tag{2a}$$

$$N_d(E)=\frac{3(E-E_v)}{2(E-E_M)}N(E) , \tag{2b}$$

$$N_p(E)=\frac{3(E-E_c)}{2(E-E_M)}N(E) , \tag{2c}$$

where N is the total DOS, N_d is the d- orbital PDOS, and N_p is the p-orbital PDOS.

These DOS functions give the number of states per unit cell per eV and include a factor of 2 for the two spin states. In Eq. (2a) K is the complete elliptic function whose argument, $W(E)$, is defined by the following relations:

$$W=[-1(\epsilon/2)^2]^{1/2} ,$$
$$\epsilon=\frac{(E-E_m)^2-(E_g/2)^2}{[(pd\pi)]^2}-2 . \tag{3}$$

Figure 3 shows the PDOS functions N_p and N_d generated from Eqs. (2a)—(2c) (solid curves) compared with the numerical results of Kopp *et al.* (dashed curves) in the energy region above 0.8 Ry. The valence-band PDOS functions from the LCAO model are also shown in the energy range below 0.8 Ry.[36]

It is important to note that the *shape* of the conduction-band PDOS functions depends on only two parameters; E_g and $(pd\pi)$. The DOS given by Eq. (2a) can accommodate six electrons and therefore is at most $\frac{1}{6}$

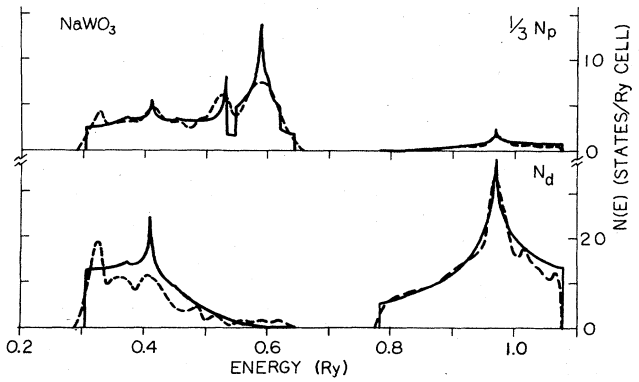

FIG. 3. Comparison of the LCAO model PDOS (solid curves) with the numerical results of energy-band calculations of Kopp *et al.* (Ref. 33). The LCAO model is described in Ref. 36.

filled for the sodium tungsten bronze alloys. Near the bottom of the conduction bands the DOS increases approximately linearly with increasing energy gap but decreases approximately quadratically with increasing $(pd\pi)$. These features can easily be seen from the expression for the jump in the DOS at the conduction-band edge, which is given by

$$N(E_c)=\frac{3E_g}{2\pi[(pd\pi)]^2} . \tag{4}$$

From the results described above it is clear that the DOS and the PDOS functions are quite sensitive to the parameters E_g and $(pd\pi)$ and that the RBM will not apply, even qualitatively, if either of these parameters change substantially with x. Consequently, it is worthwhile to consider how E_g and $(pd\pi)$ are influenced by the sodium ions.

For the purpose of discussion, let us consider the effects of the sodium concentration on Na_xWO_3 with the crystal structure constrained to be the cubic perovskite structure. In going from cubic WO_3 to $NaWO_3$, positively charged Na ions are being introduced into the lattice and, the occupation of the d orbitals increases. Changes in the electrostatic potentials occur that will significantly alter the diagonal matrix elements of the self-consistent Hartree-Fock Hamiltonian. Several experiments suggest that the band gap is increased by about 0.5 eV in going from $Na_{0.5}WO_3$ to $NaWO_3$. In optical experiments, Owen *et al.*[18] observed a shift in the peak of ϵ_2 (which we attribute to an increase in the band gap) of 0.5 eV in going from $x=0.52$ to $x=0.94$. Hollinger *et al.*[13] have estimated an increase of 0.3 to 0.4 eV in the band gap in going from $x=0.4$ t0 $x=0.83$ based on an analysis of their UPS data.

In addition to changes in the diagonal matrix elements, the off-diagonal matrix elements of the self-consistent Hamiltonian can also be expected to change with x. With increasing x, the additional electrons residing in the W $5d$ orbitals will produce a repulsive potential that will strongly affect the LCAO transfer matrix elements. Of major importance here is the effect on the transfer matrix element $(pd\pi)$, which measures the $2p-5d$ interaction strength and controls the width of the lower conduction bands. The repulsion due to the extra electrons on W ions will dominate the attractive contribution due to the positively charged Na ions because the $2p-5d$ overlap is necessarily located between the O and W ions and further removed from the Na ions. Consequently, a reduction in the $(pd\pi)$ parameter can be expected with increasing x. This mechanism for reducing $(pd\pi)$ is different from the mechanism previously suggested by Goodenough.[1] Goodenough argued that the conduction-band width would narrow due to a competition of the Na-O sigma bonding with the W-O π bonding as the sodium concentration increased. The lattice parameter of Na_xWO_3 increases with x and this effect also contributes to a decrease in $(pd\pi)$.

One effect of a $(pd\pi)$ parameter that increases with decreasing x would be to produce a smaller value of the DOS at the Fermi level for small x than would be predicted by the RBM based on the value of $(pd\pi)$ for $Na_{0.8}WO_3$. Experimentally, this effect would be most ap-

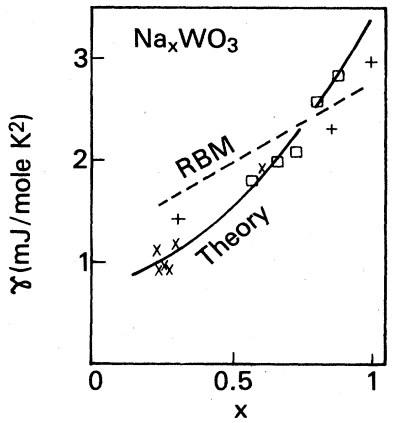

FIG. 4. Electronic specific-heat coefficient γ as a function of x for Na_xWO_3. The dashed curve is for the RBM and the solid curve is based on the model of this work. The experimental data is from Ref. 11 (+), Ref. 31 (×), and Ref. 26 (□).

parent in the electronic specific-heat coefficient γ, which is directly proportional to the DOS at the Fermi level. If $(pd\pi)$ increases with decreasing x then the RBM [with $(pd\pi)$ fixed its value for $x=0.8$] would predict values for γ which are too high for $x<0.80$ and too low for $x>0.80$. This is precisely what is observed as may be seen in Fig. 4, which shows the experimental data for γ compared with the results of the RBM. An increase in E_g with x will also contribute to this difference between experiment and theory.

In summary, theoretical considerations argue that both the band gap E_g and the interaction strength $(pd\pi)$ change significantly with sodium concentrations in Na_xWO_3 and these changes are evident in several experimental studies. The DOS and PDOS functions depend sensitively upon E_g and $(pd\pi)$ and consequently, any successful theory for Na_xWO_3 must include the x dependence of these parameters.

III. MODEL FOR THE ELECTRONIC PROPERTIES OF Na_xWO_3

The energy bands and DOS functions for the conduction bands of Na_xWO_3 are completely described by Eqs. (1) and (2a)–(2c) if the dependence of E_g and $(pd\pi)$ on x are specified. We use a simple linear interpolation scheme for both of these parameters.

For the energy gap and $(pd\pi)$ we use the relations

$$E_g(x)=2.72+x \text{ eV} , \tag{5}$$

$$(pd\pi)_x=2.44-0.86x \text{ eV} . \tag{6}$$

Equations (5) and (6) give parameters that are the same as those previously found for $x=0.8$ (see Fig. 2). The x dependence of E_g has been determined approximately by using the change in the energy gap observed in the optical experiments of Owen *el al.*[18] and the dependence of $(pd\pi)$ was determined by making use of the value of the electronic specific heat coefficient γ for $x=0.5$ (see Fig. 4).

A. Calculations of γ

The electronic specific-heat coefficient γ is given by

$$\gamma=\tfrac{1}{3}\pi^2K_B^2N(E_F)=2.362N(E_F) \text{ mj/mol K}^2 , \tag{7}$$

where E_F, the Fermi-level energy, is determined by the requirement

$$\int_{E_c}^{E_F}N(E)dE=x . \tag{8}$$

Equations (2a), (5), and (6) are used for $N(E)$, and E_F is determined from Eq. (8). The results of the calculation of γ are shown in Fig. 4 by the solid curve. It is clear that the theory agrees well with the experimental data. It is also clear that γ is not a linear function of x as has been previously suggested by several authors.[32,12] Strictly speaking our theory applies only over the range $0.5\le x\le 1$ for which Na_xWO_3 is cubic, but the results of the theory appear to agree with the data over the entire range of x.

B. Effective mass

The effective mass for electrons in Na_xWO_3 can easily be calculated from the energy-band expression of Eq. (1). For cubic Na_xWO_3 the inverse mass tensor is a multiple of the unit matrix and the diagonal elements are

$$\frac{1}{m^*}=\frac{1}{\hbar^2}\left[\frac{\partial^2E}{\partial k_\alpha^2}\right]$$

$$=\frac{4[(pd\pi)]^2a^2}{\hbar^2}\left[\frac{\cos(2k_\alpha a)}{E-E_M}-\frac{[(pd\pi)]^2\sin(2k_\alpha a)}{(E-E_M)^3}\right] . \tag{9}$$

We shall need to have the value of the inverse effective mass averaged over the Fermi surface. This quantity can easily be calculated numerically from Eq. (9). An approximate analytical expression can also be obtained by the method described below.

The average value of $\cos(2k_\alpha a)$, over the Fermi surface, can be obtained exactly:

$$\begin{aligned}\langle\cos(2k_\alpha a)\rangle&=\langle[1-2\sin^2(k_\alpha a)]\rangle\\&=1-\langle[\sin^2(k_\alpha a)+\sin^2_\beta(k_\alpha a)]\rangle\\&=1-g(E_F) ,\end{aligned} \tag{10}$$

where

$$g(E_F)=\frac{(E_F-E_m)^2-(E_g/2)^2}{4[(pd\pi)]^2} .$$

The angular brackets, $\langle\ \rangle$, in Eq. (10) indicate an average over the Fermi surface upon which the energy is E_F. The second equality of Eq. (10) is an expression of the cubic symmetry and the final result is obtained by using Eq. (1).

The average of $\sin^2(2k_\alpha a)$ cannot be obtained analytically but an excellent interpolation formula can be developed. We write

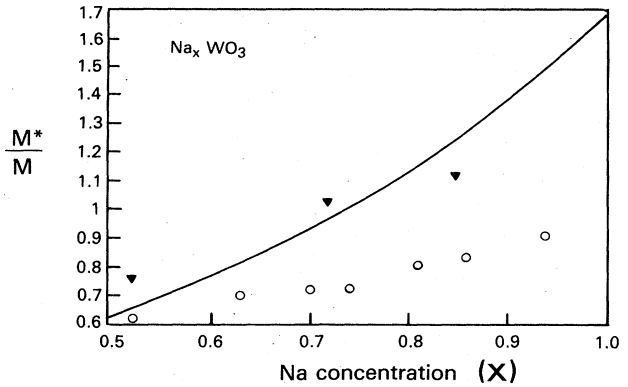

FIG. 5. Effective mass averaged over the Fermi surface as a function of x for Na_xWO_3. The solid curve is the result of the present work. The experimental data is from Ref. 18 (+) and Ref. 17 (△).

$$\tfrac{1}{4}\langle \sin^2(2k_\alpha a)\rangle$$
$$=\langle[\sin^2(k_\alpha a)-\sin^4(k_\alpha a)]\rangle$$
$$\simeq\langle \sin^2(k_\alpha a)\rangle[1-\tfrac{3}{2}(1-0.24x^6)\langle \sin^2(k_\alpha a)\rangle]$$
$$=\tfrac{1}{2}g(E_F)[1-\tfrac{3}{4}(1-0.24x^6)g(E_F)]\ . \qquad (11)$$

By combining Eqs. (10) and (11) with Eq. (9), one obtains

$$\langle m/m^*\rangle=\frac{a^2m}{\hbar^2}\left[\frac{4[(pd\pi)]^2(1-g)}{(E_F-E_M)}-\frac{8[(pd\pi)]^4g}{(E_F-E_M)^3}[(1-\tfrac{3}{4})(1-0.24x^6)g]\right]. \qquad (12)$$

In using Eq. (12) the x dependence of the W-O distance[8]

$$a=\tfrac{1}{2}(3.785+0.0818x)\ \text{Å}$$

should be employed. Equation (12) has a maximum error of 2% for $0\le x\le 1$.

The effective mass for Na_xWO_3 as a function of x has been estimated from optical data by Owen *et al.*[18] and also by Camagni *et at.*[17] A comparison of our theoretical results (solid curve) with experiments is shown in Fig. 5. Our effective-mass results compare reasonably well with those of Camagni *et al.*, but are considerably higher than those of Owen *et al.*

In view of the large discrepancies in the two sets of experimental data, a critical discussion of the differences between experiment and theory would not be very useful. However, we show in the next section that our theoretical values of the effective mass lead to predictions of the magnetic susceptibility that are in very good agreement with experimental data.

C. Magnetic susceptibility

The contribution of the conduction electrons to the magnetic susceptibility, χ in emu units is

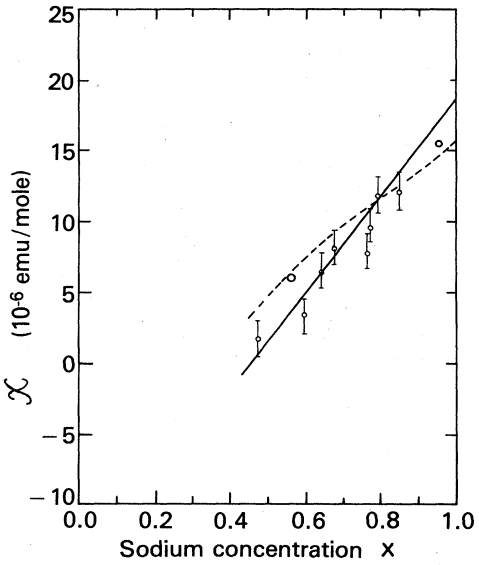

FIG. 6. Contribution of the conduction electrons to the magnetic susceptibility, χ, as a function of x for Na_xWO_3. The solid curve is the result of the present work and the dashed curve is for the rigid-band model. The experimental data is from Ref. 33 (●) and from Ref. 28 (×).

$$\chi=4.0424\times10^{-6}a^2(1-\tfrac{1}{3}\langle m/m^*\rangle^2)N(E_F)\ \text{emu/mole}\ , \qquad (13)$$

where a is the (x-dependent) W-O spacing given in the preceding section. The effective mass may be calculated numerically from Eq. (9) or the approximation given by Eq. (12) may be employed. The DOS at the Fermi energy is obtained from Eqs. (2a) and (8). The theoretical results (solid curve) are compared with the experimental data of Kupka *et al.*[28] and Greiner *et al.*[39] in Fig. 6. The dashed curve shows the results of a RBM using the DOS of Kopp *et al.* scaled to match the data at $x=0.80$. No scaling is used for our model. The agreement between our theory and experiment is quite good considering the scatter in the experimental data. On the other hand, the results of the RBM depart from the trend of the experimental data for $x<0.8$.

D. Photoemission

Approximate photoemission yield curves can be calculated from PDOS functions given by Eqs. (2b) and (2c). For the high final-state energies involved in XPS experiments the photoionization cross section for d electrons is 12 times greater than for the p electrons.[37]

The XPS photoemission intensity, $I(E)$, can be written approximately as

$$I(E)=C\int_{-\infty}^{\infty}\exp\left[\frac{E-E'}{R}\right]^2[12N_d(E')+N_p(E')]\times f(E')dE'\ , \qquad (14)$$

where C is a scale factor, $f(E')$ is the Fermi occupation

factor, and the exponential term represents the instrumental resolution function. The constant $R=0.21$ eV corresponds to a full width at half maximum (FWHM) of 0.35 eV. Including $f(E')$, the effective resolution is about 0.4 eV. (In XPS experiments the FWHM is about 0.7 eV. The value here is chosen in order to compare with the results discussed below.)

Figure 7 shows the intensity curves predicted by Eq. (14) for several values of x. For these curves the top of the valence band is fixed at an energy of -8.75 eV. The FWHM for the emission curves, 1.0, 1.0, 1.0, and 0.9 eV for $x=0.83$, 0.73, 0.62, and 0.4, respectively, is surprisingly constant. This effect may offer an explanation of the UPS results of Höchst *et al.*,[12] who reported that the FWHM was constant at 1 eV independent of x.

Hollinger *et al.*[13] recently reported synchrotron radiation UPS photoemission results for Na_xWO_3 for $0.4 \leq x \leq 0.85$. They argued that the intensity curves follow the gross physical features of the RBM. In Fig. 8 the results of our model are compared with the experimental results of Hollinger *et al.* The scale factor, C, of Eq. (14) was chosen so that the theoretical peak intensity matches the experimental peak for $x=0.4$. All other factors are known. The areas under the theoretical curves agree very well with the areas under the corresponding experimental curves even though no effect was made to normalize the areas.

The agreement between our theory and experiment is quite reasonable considering that strong transition matrix elements that modulate the UPS intensity curves. Phonon scattering and plasmon effects contribute to the intensity in the band-gap region and lead to a broadening of the experimental curves on the low-energy side, which is not present in the theoretical curves. In addition, the photoinization cross sections for the p and d electrons are more nearly equal in these UPS experiments.

Hollinger *et al.*[13] also present photoemission curves using the RMB and the results of Kopp *et al.* The agreement between the RBM and experiment is similar to what is seen for our theory in Fig. 8. This underlines the fact that data arising from conduction-band photoemission alone is *not* sufficiently accurate to distinguish between the two different band models. This point has been emphasized earlier by Wertheim *et al.*[10]

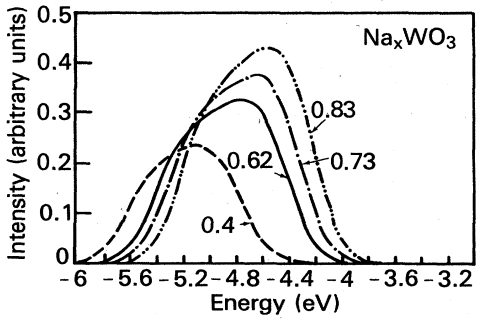

FIG. 7. Theoretical distribution curves for XPS photoemission from the conduction bands of Na_xWO_3 for $x=0.4$, 0.62, 0.73, and 0.83. The energy of the top of the valence band is taken to -8.75 eV.

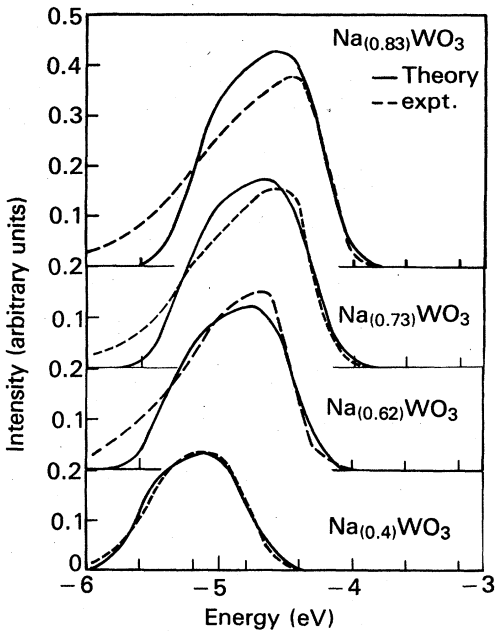

FIG. 8. Comparison of the theoretical and experimental (Ref. 13) photoemission energy distribution curve for several values of x.

E. Optical properties

Owen *et al.* observed a shift in the peak of the imaginary part of the dielectric constant, ϵ_2, of 0.5 eV in going from $x=0.52$ to $x=0.94$. The half- maximum intensity point in ϵ_2 increases from 4 to 4.5 eV.

Owen *et al.* attribute the peak in ϵ_2 to transitions from the top of the valence band to the peak in the DOS of the conduction band. We shall argue that this interpretation is incorrect and that the peak in ϵ_2 is associated with transitions from top of the valence band to empty states above the Fermi level.

According to our model there is a significant narrowing of the t_{2g}-band width with increasing x. In going from $x=0.52$ to $x=0.94$, for example, the width decreases from 4.3 to 3.13 eV. As the band narrows the peak in the DOS necessarily moves *closer* to the bottom of the conduction band. Therefore, the shift is in the opposite direction from that observed ob Owen *et al.* as shown in Fig. 9.

The model gives the energy from the top of the valence band to the peak in the DOS to be 5.92 eV for $x=0.52$ and 5.57 eV for $x=0.94$. These energies are far too large to explain the experimental results of Owen *et al.*

On the other hand, the energy difference between the top of the valence band and the Fermi energy is 4.17 eV for $x=0.52$ and 4.63 eV for $x=0.94$. These energies and the shift of 0.46 eV are very close to those observed by Owen *et al.*

The question arises as to why ϵ_2 does not show a peak due to transitions of the type supposed by Owen *et al.* The answer is that the matrix elements for transitions from the top of the valence band to the t_{2g} band decrease rapidly with increasing transition energy. (We have given

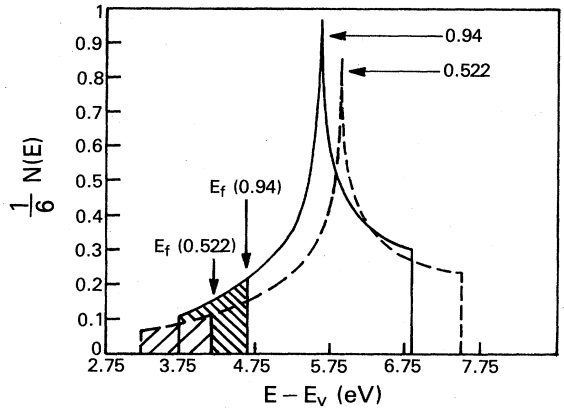

FIG. 9. DOS for the conduction band for $x=0.522$ and $x=0.94$ for Na_xWO_3. The shaded regions indicate the occupied states.

a detailed discussion of this effect in a previous paper[40]). This decrease in transition strength with increasing energy is also apparent in the data of Owen *et al.*

F. Neutron scattering data

Kamitakahara *et al.*[41] reported inelastic neutron scattering measurements of the Kohn anomaly in the longitudinal-acoustic-phonon branch of Na_xWO_3 for $x=0.56$, 0.59, and 0.83. The Kohn anomaly appears as a kink in the phonon dispersion curve along the $\Gamma-X$ direction. The phonon wave vector at which the kink occurs is twice the magnitude of the Fermi wave vector according to Kamitakahara *et al.* From experiments they deduce the values of $(2k_fa/\pi)$ to be 0.315, 0.345, and 0.395 ± 0.010 for $x=0.56$, 0.59, and 0.83, respectively. Using the model described in this paper we find the values 0.342, 0.354, and 0.415 for the same x values listed above. Our values are 8.5%, 2.6%, and 5% higher, respectively, than those given by Kamitakahara *et al.* (who suggest an experimental uncertainty of $\pm2\%$) and are 3% higher than the RBM results in all cases.

IV. CONCLUSIONS

In the preceding section we presented a simple semiempirical LCAO model which describes in detail the x-dependent electronic properties of cubic Na_xWO_3 for $0.5\leq x\leq 1$. The variation in the energy gap and the p-d interaction strength that is found is large enough to rule out the use of the RBM.

We presented closed-form analytical expressions for the conduction-energy bands, total density of states, p and d orbital partial density-of-state functions, effective mass, specific-heat coefficient, and magnetic susceptibility. We demonstrated good agreement between the predictions of our model and the experimental data for XPS and UPS photoemission and for the electronic specific heat, magnetic suscepticility, and the optical dielectric constant.

Because of the simplicity of our model one cannot expect to produce highly accurate results. However, the uncertainties in experimental data are far larger than any error associated with the model.

The principal value of the model is that it reveals the dependence of the electronic properties on the few physically meaningful parameters and consequently provides considerable insight into the electronic properties of the sodium tungsten bronze compounds. In addition, the utility of the model for interpreting experimental data is clearly demonstrated.

[1]J. B. Goodenough, Prog. Solid State Chem. **5**, 195 (1971).
[2]A. Ferreti, D. B. Rogers, and J. B. Goodenough, J. Phys. Chem. Solids **26**, 2007 (1965).
[3]N. F. Mott, Philos. Mag **35**, 111 (1977).
[4]C. J. Raub, A. R. Sweedler, M. A. Jensen, S. Broadston, and B. T. Matthias, Phys. Rev. Lett. **13**, 746 (1964).
[5]H. R. Shanks, Solid State Commun, **15**, 753 (1974).
[6]K. L. Ngai and R. Silberglitt, Phys. Rev. B **13**, 1032 (1976).
[7]G. Hagg, Z. Phys. Chem. Abt. B **29**, 192 (1935).
[8]B. W. Brown and E. Banks, J. Am. Chem. Soc. **76**, 963 (1954).
[9]J. N. Chazalviel, M. Campagna, G. K. Wertheim and H. R. Shanks, Phys. Rev. B **16**, 697 (1977).
[10]G. K. Wertheim and J. N. Chazalviel, Solid State Commun. **40**, 931 (1981).
[11]H. Höchst, R. D. Bringans, H. R. Shanks, and P. Steiner, Solid State Commun. **37**, 41 (1980).
[12]H. Höchst, R. D. Bringans, and H. R. Shanks, Phys. Rev. B **26**, 1702 (1982).
[13]G. Hollinger, F. J. Himpsel B. Reihl, P. Pertose, and J. P. Doumerc, Solid State Commun. **44**, 1221 (1982).
[14]R. G. Egdell and M. D. Hill, Chem. Phys. Lett. **85**, 140 (1982).
[15]T. Wolfram and S. Ellialtioglu, Phys. Rev. B **19**, 43 (1979).
[16]M. Campagna, G. K. Wertheim, H. R. Shanks, F. Zumsteg, and E. Banks, Phys. Rev. Lett. **34**, 738 (1975).
[17]P. Camagni, A. Manara, G. Campagnoli, A. Gustinetti, and A. Stella, Phys. Rev. B **15**, 4623 (1977).
[18]J. F. Owen, K. J. Teegarden, and H. R. Shanks, Phys. Rev. B **18**, 3827 (1978).
[19]P. G. Dickens, R. M. P. Quillam, and M. S. Whittingham, Mater. Res. Bull. **3**, 941 (1968).
[20]G. H. Taylor, J. Solid State Chem. **1**, 359 (1969).
[21]S. Fujieda, Sci. Light (Tokoyo) **18** (1969).
[22]F. Consadori and A. Stella, Nuovo Cimento Lett. **3**, 600 (1970).
[23]G. Giuliani, A. Gustinetti, and A. Stella, Phys. Lett. **38A**, 515 (1972).
[24]D. W. Lynch, R. Rosei, J. H. Weaver, and C. G. Olson, J. Solid State Chem. **8**, 242 (1943).
[25]J. Feinleib, W. J. Scouler, and A. Ferretti, Phys. Rev. **165**, 765 (1968).
[26]R. W. Vest, M. Griffel, and J. F. Smith, J. Chem. Phys. **28**, 293 (1958).
[27]W. R. Gardner and G. C. Danielson, Phys. Rev. **93**, 46 (1954).
[28]F. Kupka and M. J. Sienko, J. Chem. Phys. **18**, 1296 (1950).
[29]P. M. Stubbin and D. P. Mellor, J. R. Soc. New South Wales

82, 225 (1948).
[30]B. L. Crowder and M. J. Sienko, J. Chem. Phys. **38**, 1576 (1963).
[31]L. D. Muhlstein and G. C. Danielson, Phys. Rev. **158**, 852 (1967); **160**, 562 (1967); H. R. Shanks, P. H. Sidles, and G. C. Danielson, Adv. Chem. **39**, 237 (1963); L. D. Ellerbeck, H. R. Shanks, P. H. Sidles, and G. V. Danielson, J. Chem. Phys. **35**, 298 (1961).
[32]C. Zumsteg, Phys. Rev. B **14**, 1401 (1976).
[33]L. Kopp, B. N. Harmon, and S. H. Liu, Solid State Commun. **22** 677 (1977).
[34]R. Clark, Phys. Rev. Lett. **39**, 1550 (1977).
[35]T. Wolfram, E. A. Kraut, and F. J. Morin, Phys. Rev. B **7**, 1677 (1973).
[36]T. Wolfram and S. Ellialtioglu, Phys. Rev. B **25**, 2697 (1981).
[37]T. Wolfram and S. Ellialtioglu, Phys. Rev. B **19**, 43 (1979).
[38]T. Wolfram, Phys. Rev. Lett. **29** 1383 (1972).
[39]J. D. Greiner, H. R. Shanks, and D. C. Wallace, J. Chem Phys. **36** 772 (1962).
[40]T. Wolfram and S. Ellialtioglu, Appl. Phys. **22**, 11 (1980).
[41]W. A. Kamitakahara, B. N. Harmon, J. G. Taylor, L. Kopp, H. R. Shanks, and J. Roth, Phys. Rev. Lett. **36**, 1393 (1976).